Submitted to

International Europhysics Conference on High Energy Physics, July 12, 2001, Budapest
EPS 2001: Abstract: **796**
Parallel Session **Soft Interactions, Hadronic Structure and Diffraction**

XX International Symposium on Lepton and Photon Interactions, July 23, 2001, Rome
LP 2001: Abstract: **489**
Parallel Session **s08**

www-h1.desy.de/h1/www/publications/conf/conf_list.html

Measurement of density matrix elements for ρ meson production as a function of t at HERA

H1 Collaboration

Abstract

A sample of $e^+\pi^+\pi^-$ events with $Q^2 > 2.5\ \mathrm{GeV}^2$, $40 < W < 120$ GeV and $t' = |t| - t_{min}$ in the range $0.5 < t' < 3.0\ \mathrm{GeV}^2$ is used to measure the r^{04}_{00} density matrix element and the combinations $r^5_{00} + 2r^5_{11}$ and $r^1_{00} + 2r^1_{11}$. The t' dependences are determined.

1 Introduction

The mechanism of diffraction, especially in a QCD approach, can in particular be studied through the diffractive electroproduction of vector mesons (VM) at high energy:

$$e + p \to e + VM + Y, \tag{1}$$

where Y is a proton ("elastic" scattering) or a baryonic system of mass M_Y much lower than the invariant mass W of the hadronic system: $M_p < M_Y \ll W$ ("proton dissociation" scattering).

The measurement of the production and decay angle distributions of the vector meson provides information on the angular momentum structure of the interaction. Detailed results have been reported on the spin density matrix elements for ρ and ϕ elastic electroproduction with $|t| < 0.5$ GeV^2 [1, 2, 3], t being the square of the four-momentum transferred to the proton, and for ρ electroproduction with proton dissociation for $t' < 1.5$ GeV^2 [4], where t' is defined as $t' = |t| - t_{min}$, t_{min} being the minimal value of $|t|$ kinematically required to put the vector meson and the system Y on shell. This variable is more relevant than t when M_Y and/or the photon virtuality are not negligible with respect to W.

Three main features emerge from these measurements [1]

- the dominance of the longitudinal T_{00} over the transverse T_{11} helicity non-flip amplitudes for $Q^2 \gtrsim 1$ GeV^2 (Q^2 is the negative square of the virtual photon four-momentum), as measured by the r^{04}_{00} density matrix element in the s-channel helicity conservation (SCHC) approximation;
- the presence of a small but significant violation of SCHC, revealed by the non-zero value of the r^5_{00} matrix element, which indicates that the dominant helicity flip amplitude is from a transverse photon to a longitudinal vector meson ($T_{01} \neq 0$);
- values compatible with zero for the other amplitudes describing single or double helicity flip.

[1] The following relations [5] between density matrix elements and helicity amplitudes $T_{\lambda_\rho \lambda_\gamma}$ are relevant for the present analysis, natural parity exchange being assumed to hold ($T_{-\lambda_\rho - \lambda_\gamma} = (-1)^{\lambda_\rho - \lambda_\gamma}\, T_{\lambda_\rho \lambda_\gamma}$):

$$\begin{aligned}
r^{04}_{00} &\propto \frac{|T_{00}|^2 + |T_{01}|^2}{N} \\
r^5_{00} &\propto \frac{1}{N} \mathrm{Re}\,(T_{00}\, T^\dagger_{01}) \\
r^5_{11} &\propto \frac{1}{N} (\mathrm{Re}\,(T_{10} T^\dagger_{11}) - \mathrm{Re}\,(T_{10} T^\dagger_{1-1})) \\
r^1_{00} &\propto \frac{-1}{N} |T_{01}|^2 \\
r^1_{11} &\propto \frac{1}{N} (T_{1-1} T^\dagger_{11} + T_{11} T^\dagger_{1-1}) \\
\text{with } N &= \sum_{i,j} |T_{ij}|^2 \ , \ \ i = \lambda_\rho, j = \lambda_\gamma \ \ = -1, 0, 1
\end{aligned} \tag{2}$$

These general features are in agreement with perturbative QCD calculations [2] [6, 7, 8]. In addition, the following amplitude hierarchy is predicted for moderate Q^2 and t: $|T_{00}| > |T_{11}| > |T_{01}| > |T_{10}| > |T_{1-1}|$, the r^1_{00} density matrix element is expected to be slightly negative, and the following t dependences are predicted for amplitude ratios: a constant ratio for helicity conserving amplitudes, a $\sqrt{|t|}$ dependence for the ratio of the single helicity flip to the non-flip amplitudes, and a linear dependence for the ratio of the double flip to the non-flip amplitudes.

The present paper deals with the measurement, as a function of t', of density matrix elements for ρ meson diffractive electroproduction:

$$e + p \rightarrow e + \rho + Y; \quad \rho \rightarrow \pi^+\pi^-, \tag{3}$$

in the kinematic domain defined as:

$$\begin{aligned} 2.5 < Q^2 &< 30 \text{ GeV}^2 \\ 40 < W &< 120 \text{ GeV} \\ 0.5 < t' &< 3 \text{ GeV}^2 \\ E - p_z &> 52 \text{ GeV} \\ 0.6 < M_\rho &< 1.1 \text{ GeV} \\ M_Y &< 25 \text{ GeV}, \end{aligned} \tag{4}$$

thus extending the t' range of ref. [1, 2, 3, 4].

The ρ meson mass M_ρ is reconstructed as the invariant mass $M_{\pi\pi}$ of the two charged pion candidates, and the ρ momentum is computed as the sum of the pion candidate momenta. The variable t' is determined from the scattered electron and charged pion momentum components transverse to the beam direction, as

$$t' = (\bar{p}^T_{miss})^2 = (\bar{p}^T_e + \bar{p}^T_\rho)^2, \quad \bar{p}^T_\rho = \bar{p}^T_{\pi^+} + \bar{p}^T_{\pi^-}. \tag{5}$$

The variable $E - p_z$ is the difference of the energies and the longitudinal momenta of the scattered electron and the ρ meson candidate.

The t' distribution in diffractive ρ electroproduction is exponentially falling: $\mathrm{d}\sigma/\mathrm{d}t' \propto e^{-b \cdot t'}$, with $b \simeq 7 \text{ GeV}^{-2}$ for elastic scattering [1] and $b \simeq 2.5 \text{ GeV}^{-2}$ for proton dissociative scattering [4], in the Q^2 range relevant for the present analysis. Because of the very small cross section at large t', a major difficulty of the analysis is the presence of vector mesons produced at low t', but faking ρ production at higher t'. An example is low t' electroproduction of ρ' mesons [3] decaying into two charged pions and two π^0's:

$$\rho' \rightarrow \rho^+\pi^-\pi^0, \quad \rho^+ \rightarrow \pi^+\pi^0 \quad (+\ c.c.). \tag{6}$$

This process mimics channel (3) when the $\pi^+\pi^-$ invariant mass is in the ρ mass range and the decay photons of the π^0's remain undetected, which happens if they are associated with the

[2] In Ref. [6], perturbative QCD calculations are assumed to be valid for $|t| \leq Q^2\gamma$, where γ is the gluon anomalous dimension, depending on Q^2 and the energy. Strictly speaking, the predictions are for elastic scattering.

[3] The detailed structure [9] of the states previously described as the $\rho'(1600)$ meson is not relevant for the present study. The name ρ' is thus effectively used for the vector meson state combination of mass in the range 1450-1700 MeV and width of the order of 150 MeV.

charged pion candidate tracks or do not pass the detection threshold in the detector. In such a case, the p^T unbalance of the event due to the loss of the π^0's is interpreted as ρ production at high t' following eq. (5). In spite of the very small probability for the four decay photons to remain undetected, it will be shown below that this channel gives a non-negligible background to large t' ρ production. Similar cases are ω and ϕ production

$$\omega \to \pi^+\pi^-\pi^0,$$
$$\phi \to K_S^0 K_L^0, \quad \phi \to \pi^+\pi^-\pi^0, \tag{7}$$

when the π^0 or the K_L^0 remains undetected. Note however that these channels mostly give contributions below the selected ρ mass range.

In the following, any diffractive background of type $\pi^+\pi^- X^0$, where X^0 only contains neutral particles, will be generically attributed to ρ' production, unless otherwise stated in the case of processes (7).

2 Event selection, kinematic variables and simulations

The data used for the present analysis were taken with the H1 detector in 1997 (more details for the relevant parts of the detector can be found in [1]). The energies of the HERA proton and positron beams [4] were respectively 820 and 27.5 GeV, and the integrated luminosity used for the analysis amounts to 6.0 pb^{-1}.

Events corresponding to channel (3), in the kinematic range defined by relations (4), were selected by requesting the reconstruction of a cluster with energy larger than 17 GeV in the SpaCal backward electromagnetic calorimeter [5], and the reconstruction in the central tracking detector of the trajectories of two and only two charged particles (pion candidates) with opposite charges, momenta larger than 0.1 GeV and polar angles confined within the interval $20 < \theta < 160^o$. Reconstructed energy clusters in the electromagnetic (hadronic) part of the liquid argon (LAr) calorimeter surrounding the tracker were associated with pion candidates when the cluster distance to the extrapolated particle direction was smaller than 40 (60) cm. The event was rejected if at least one cluster was reconstructed with energy larger than 400 MeV (300 MeV) in the LAr (SpaCal) calorimeter, and was not associated with a charged pion candidate; LAr energy clusters in the forward direction, which could be attributed to products of proton dissociation, were not included in this rejection criterium.

Events were classified in two categories, corresponding to the presence or absence of activity in the forward detectors. A selected event was classified in the "notag" sample when no signal was detected neither in the proton remnant tagger (PRT), nor in the forward muon detector (FMD), no track was reconstructed with polar angle $\theta < 20^o$ and no cluster with energy larger than 400 MeV was detected in the LAr calorimeter. Conversely, events were classified in the "tag" sample if a signal was observed in either the PRT or the FMD, if a track was reconstructed with polar angle $\theta < 20^o$ or if a cluster with energy larger than 400 MeV was reconstructed in

[4] In the following, the word electron will be used for both electrons and positrons.

[5] In the H1 convention, the z axis is defined by the colliding beams, the forward direction being that of the outgoing proton beam and the backward direction, that of the electron beam.

the forward part of the LAr. A pseudorapidity interval of at least 2.2 units was required between the edge of the LAr calorimeter or the most backward track or cluster attributed to proton dissociation, and the most forward charged pion candidate.

These two samples could be attributed, to first approximation, respectively to the elastic and the proton dissociation processes. However, elastic events are classified in the tag sample if t is large enough that the scattered proton hits the beam pipe walls or adjacent material, giving a signal in the forward detectors, or in the case of noise in the forward detectors. Conversely, proton dissociation events can be classified in the notag sample in the case of a small mass M_Y and/or inefficiency of the forward detectors.

For the present analysis, it is thus important to recognize that proton dissociation and elastic ρ events at large t' mostly belong to the tag sample, whereas low t' background events, as in processes (6,7), belong to either the tag or the notag sample, depending on the proton dissociation to elastic cross section ratio and on the detector response. The fraction of ρ' background is thus smaller in the tag sample, which will be used for the extraction of density matrix elements.

The variable Q^2 is reconstructed (double angle method) as:

$$Q^2 = \frac{4{E_o}^2 \ \sin\theta_\rho \ (1+\cos\theta_e)}{\sin\theta_e + \sin\theta_\rho - \sin(\theta_e+\theta_\rho)}, \tag{8}$$

where E_o is the energy of the incoming electron, and θ_e and θ_ρ are the scattered electron and ρ meson polar angles. The variable W is given by (Jacquet-Blondel method):

$$W^2 = y \cdot s - \frac{{p_\rho^T}^2}{1-y}, \qquad y = \frac{E_\rho - p_{z\rho}}{2E_o}, \tag{9}$$

s being the square of the ep centre of mass energy. For computing t' according to eq. (5), the electron momentum is computed using the ρ momentum and the electron polar angle. For $E - p_z$, the electron energy measured in the SpaCal is used. Fig. 1 presents the t' distribution for the selected tag events.

The angles θ^* and Φ, used for the extraction of the density matrix elements [1, 5], are measured using the event kinematics defined by equations (8) and (9): θ^* is the angle between the π^+ and ρ meson directions in the ρ rest frame, Φ is the angle between the ρ production plane and the electron scattering plane in the (γp) centre of mass system.

Monte Carlo simulations based on the DIFFVM program [10] are used to describe the elastic and proton dissociation production of ρ, ω, ϕ and ρ' vector mesons, and to correct the signal for acceptance and smearing effects.

For ρ production, the simulations include the angular distributions (see definitions in [1, 5]) corresponding to the measurements of the present analysis for the r^{04}_{00} matrix element ($\cos\theta^*$ distribution) and the $r^5_{00} + 2r^5_{11}$ and $r^1_{00} + 2r^1_{11}$ combinations (Φ distribution). Other angular distributions and correlations are taken in the s-channel helicity conservation approximation, the interference between the longitudinal and transverse amplitudes ($\cos\delta$ parameter) being taken from the elastic scattering measurement [1] in the relevant Q^2 range. Radiative effects [11] are fully included, and the measurements below include radiative corrections. For $t' > 0.5~\mathrm{GeV}^2$, the t' slope is taken to be $b = 7~\mathrm{GeV}^{-2}$ for elastic scattering [1] and $b = 1.7~\mathrm{GeV}^{-2}$ for proton

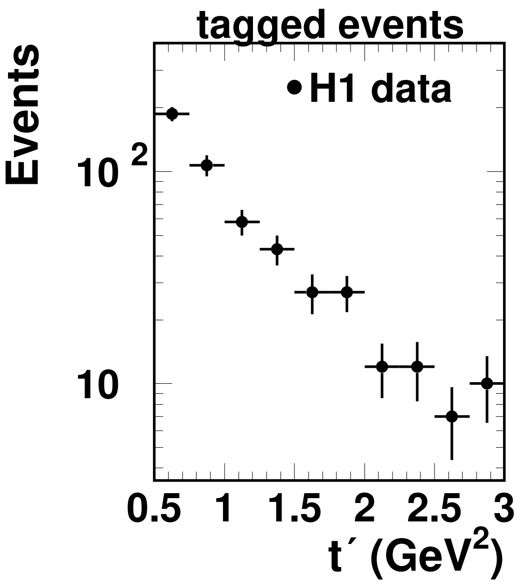

Figure 1: Uncorrected t' distribution for the selected tag events in the range 0.5-3.0 GeV^2

dissociation scattering. The t' integrated cross section ratio for proton dissociation and elastic scattering is taken as 0.95. All parameters in the simulation can be varied.

For ω, ϕ and ρ' production in channels (6,7), the decay angular distributions have not been measured, and are taken isotropic. The t' slopes are $b = 6\ \mathrm{GeV}^{-2}$ for elastic scattering and $b = 2.5\ \mathrm{GeV}^{-2}$ for proton dissociation. The ratio of the proton dissociation to elastic channels, integrated over t', is taken to be 0.75. For the present Q^2 range, the ratio of the ω to ρ and of the ϕ to ρ production cross sections, integrated over t' and over the full ρ mass range, are taken to be 0.09 [12] and 0.20 [3], respectively. The ρ' to ρ cross section ratio is not measured. It is extracted from the present data in the mass range $0.6 < M_\rho < 1.1$ GeV and for $0.5 < t' < 3$ GeV^2.

3 Signal extraction and matrix element measurements

3.1 Backgrounds

To estimate the background contributions, a new variable, ζ, is introduced:

$$\zeta = \cos{(p^T_{miss},\ p^T_\rho)}. \tag{10}$$

For ρ' production [6], p^T_{miss} is mostly due to the non-detection of the decay photons of the π^0's, which induces p^T unbalance. In the present Q^2 range, the π^0's are mostly emitted in the (π^+, π^-) direction, giving a ζ distribution peaking around +1. In contrast, in the case of high t' ρ production, p^T_{miss} is due to the scattered proton or system Y, leading to a more symmetric distribution, peaking at +1 and -1.

[6] Here "ρ'" is generically used for any diffractive system containing two charged and additional neutral particles.

The selected events are distributed in 4 subsamples: tag and notag events, with $\zeta < 0$ or with $\zeta > 0$. Each of these 4 samples contains 2 contributions, due respectively to ρ production at large t', and to the ρ' background.

In addition to the conservation of the total number of events, 6 constraints are obtained from the Monte Carlo simulations:

- the fractions of ρ events with $\zeta < 0$, respectively for the tag and notag samples, as obtained from the ζ distributions in the ρ simulation;
- similarly, the fractions of ρ' events with $\zeta < 0$, as obtained from the ρ' simulation;
- the fraction of tagged ρ' events, for $\zeta < 0$ and $\zeta > 0$, respectively. These fractions are obtained from the detector simulation, under the assumption that the ratio of proton dissociation to elastic ρ' production cross sections is 0.75.

The ρ and ρ' contributions are then determined through a global fit of the numbers in the 4 samples under the 6 constraints, performed with the MINUIT package [13]. As expected, the amount of ρ' background is significantly smaller in the tag sample.

However, the ζ distribution in the ρ simulation used for the constraint calculation is related to the Φ angle distribution, which in turn depends on the input density matrix elements as:

$$W(\Phi) \propto 1 + \sqrt{2\epsilon(1+\epsilon)}\ \cos\Phi\ (r^5_{00} + 2r^5_{11}) - \epsilon\ \cos 2\Phi\ (r^1_{00} + 2r^1_{11}), \tag{11}$$

where the polarisation parameter $\epsilon = 0.99$ in the HERA range.

The measured Φ distribution for the tag sample, corrected for the ρ' background and for acceptance and smearing effects, is fitted to relation (11). The extracted values for the density matrix element combinations $r^5_{00} + 2r^5_{11}$ and $r^1_{00} + 2r^1_{11}$ are then fed back into the ρ simulation. The new ζ distribution provides a modified constraint, and the fit procedure is iterated. The process converges after a few steps to stable background estimates and is independent of the starting value of the density matrix elements in the ρ Monte Carlo.

Fig. 2a, c, e and g presents the $\pi^+\pi^-$ mass distribution over the full mass region $0.3 < M_{\pi\pi} < 1.3$ GeV for the tag sample, the notag sample, the $\zeta < 0$ and $\zeta > 0$ sample respectively. The background contributions are also shown. Fits of the background subtracted distributions to relativistic Breit-Wigner functions with the Ross-Stodolsky skewing parameter [14] fixed to 1 [1], yield ρ mass and width values in agreement with expectations [9] (see Fig. 2b for the tag sample, and d, f and g for the other samples). The data are thus very well described over the full mass range by the diffractive ρ production at large t' supplemented by ω, ϕ and ρ' backgrounds.

3.2 $(r^5_{00} + 2r^5_{11})$ and $(r^1_{00} + 2r^1_{11})$ determination

Once the iterative process described above has converged, measurements for the density matrix element combinations $r^5_{00} + 2r^5_{11}$ and $r^1_{00} + 2r^1_{11}$ are obtained from the Φ distribution in two bins in t': $0.5 < t' < 1.0$ GeV^2 and $1.0 < t' < 3.0$ GeV^2.

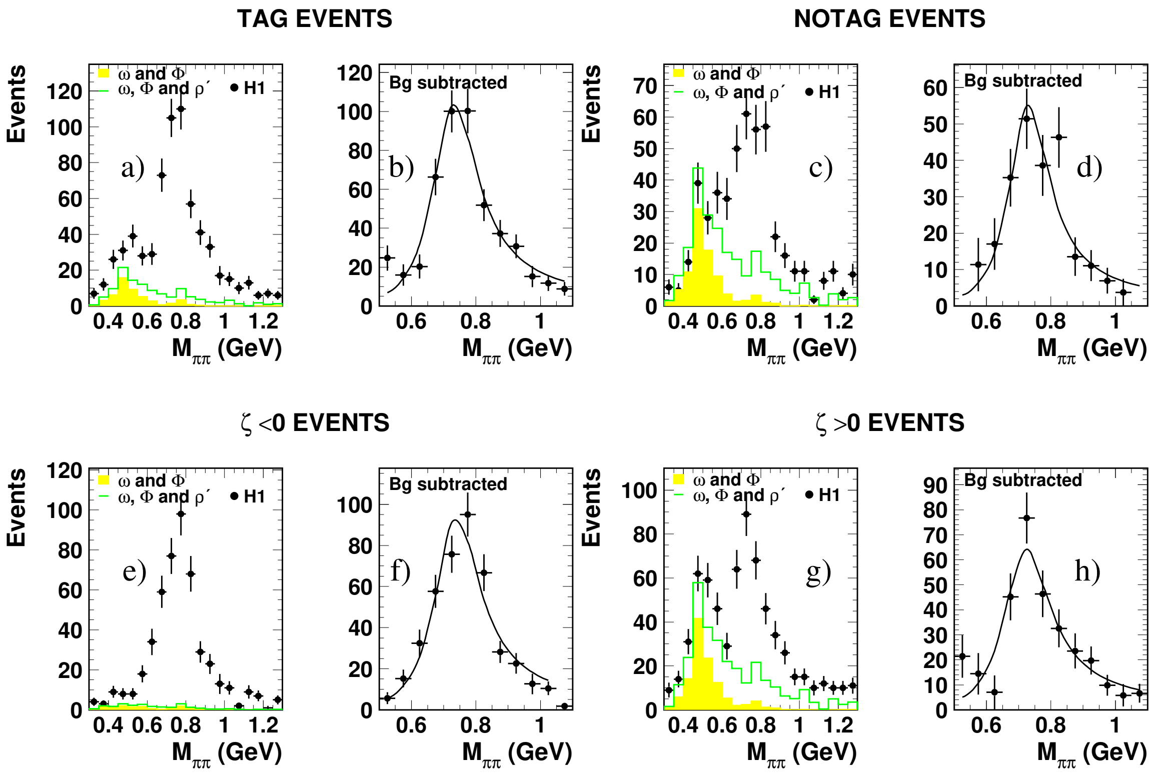

Figure 2: a-c-e-g) $\pi^+\pi^-$ mass distributions for the selected events with $0.3 < M_{\pi\pi} < 1.3$ GeV; the dark histograms describe the ω and ϕ background contributions, while the full histograms include the additional ρ' background , b-d-f-h) background subtracted $M_{\pi\pi}$ distributions, the curves being the result of fits to a relativistic Breit-Wigner distribution with the Ross-Stodolsky parameter fixed to 1. The plots a and b are for the tag events, c and d for the notag events, e and f for the $\zeta < 0$ sample and g and h for the $\zeta > 0$ sample.

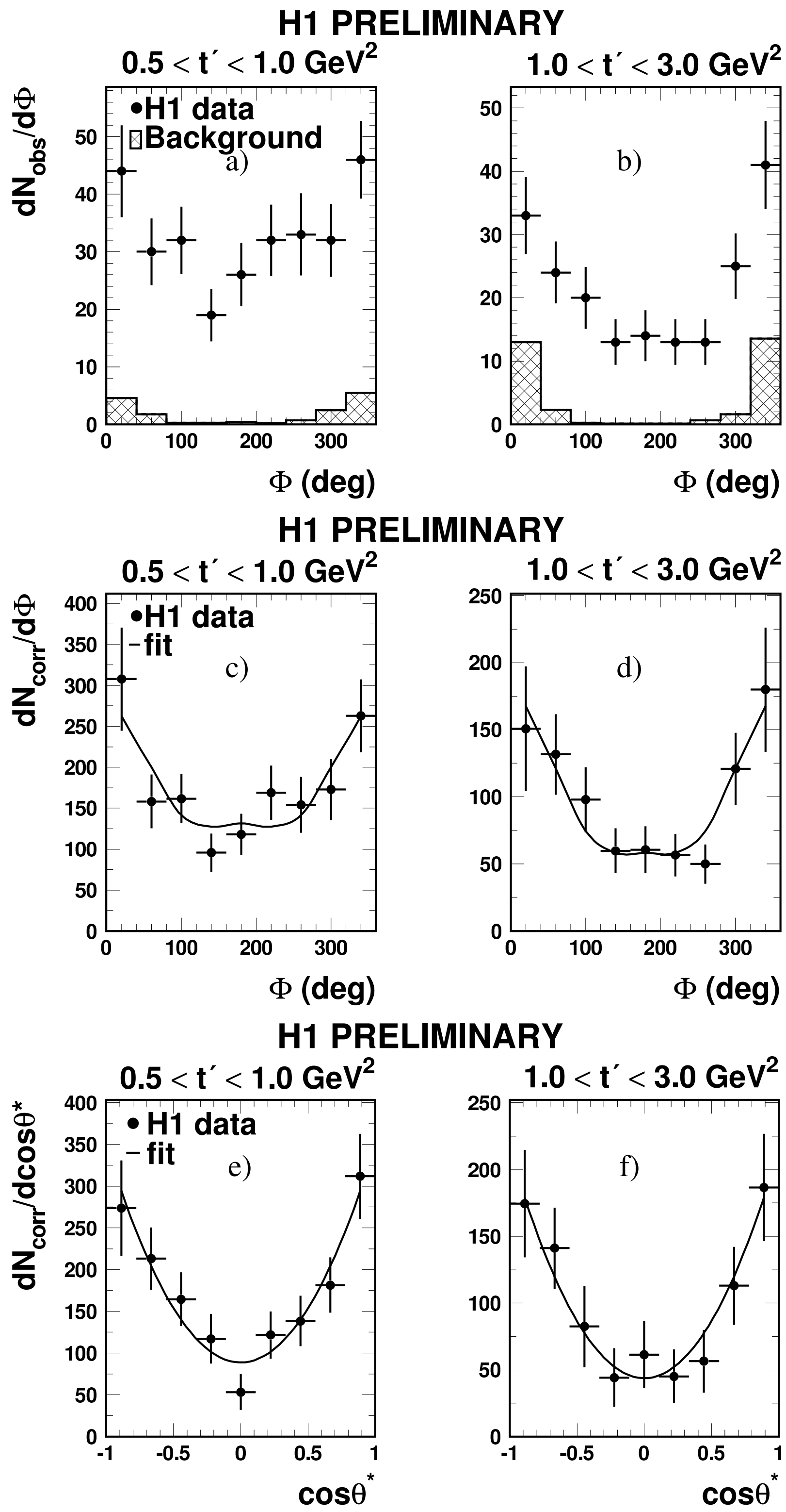

Figure 3: a-b) Observed Φ distributions for the tag events; the hatched area describes the final estimate of the backgrounds. c-d) Fully corrected Φ distributions for the tag sample; the superimposed curves show the results of fits to relation (11). e-f) Fully corrected $\cos\theta^*$ distributions for the tag sample; the superimposed curves show the results of fits to relation (12). The plots a-c-e are for $0.5 < t' < 1.0$ GeV^{2}and b-d-f are for $1.0 < t' < 3.0$ GeV^2.

Fig. 3a-b presents the observed Φ distributions of the tag events for the two bins in t', including the final estimates of the background. Fig. 3c-d shows the fully corrected distributions used to determine the density matrix element combinations.

To compute the errors on the measurement, several uncertainties were considered:

- the uncertainty of the amount of background was estimated by varying, for the fit procedure, the ζ separation between the samples from 0.0 to ± 0.2 and ± 0.4;
- the fractions of ρ' events with $\zeta < 0$ were multiplied by factors 2 and 0.5;
- the proton dissociative to elastic ρ' production cross section ratio was changed to 0.5 and to 1.0;
- the Φ shape of the background was varied by keeping the total amount fixed, but changing the fraction assigned to the two extreme Φ bins by ± 50 %;
- the energy threshold for the detection of clusters not associated to tracks in the LAR calorimeter was varied between 300 MeV and 500 MeV;
- the efficiencies of the PRT and FMD were varied within experimental errors;
- the M_Y spectrum was varied from $1/M_Y^{2.15}$ to $1/M_Y^{1.85}$ and to $1/M_Y^{2.45}$.

For each of these variations, the full iterative procedure was performed. The spread of results was quadratically combined with the statistical errors from the fit to relation (11) to determine the total errors on the measurements.

The values obtained for the density matrix element combinations $r^5_{00} + 2r^5_{11}$ and $r^1_{00} + 2r^1_{11}$ are presented in fig. 4a and 4b, respectively, together with measurements at lower t' values in similar energy and Q^2 ranges ($Q^2 > 2.5$ GeV^2 for ref. [1], $Q^2 > 1.5$ GeV^2 for ref. [4] and $Q^2 > 3.0$ GeV^2 for ref. [2]).

Significant helicity non-conservation is observed for the combination $r^5_{00} + 2r^5_{11}$. Following the results of [1, 2], this effect is mainly attributed to the r^5_{00} density matrix element, which is proportional to the product of the dominant non-flip amplitude T_{00} by the amplitude T_{01}, which is expected to be the largest helicity flip amplitude. In contrast, the r^5_{11} density matrix element has a contribution from the product of the non-dominant non-flip amplitude T_{11} by the non-dominant single flip amplitude T_{10}, plus a contribution from double flip. A fit to the measurements of the present analysis, together with those of ref. [1] which were obtained in the same Q^2 range, is performed assuming a dependence of the type $\sqrt{t'}$ [6]. The data are compatible with this dependence, the result of the fit being $r^5_{00} + 2r^5_{11} = (0.25 \pm 0.03)\,\sqrt{t'}$, with t' in GeV^2; the full errors on the measurements are used to estimate the fit error. The present analysis is the first measurement of this dependence.

In fig. 4b, the values found for $r^1_{00} + 2r^1_{11}$ are shown; they are different from zero and negative. The present measurement is the first observation of a significant non-zero value of the $r^1_{00} + 2r^1_{11}$ density matrix element combination. The r^1_{00} element, which is expected to give a negative contribution [6], is proportional to the square of the single flip amplitude T_{01}. The r^1_{11}

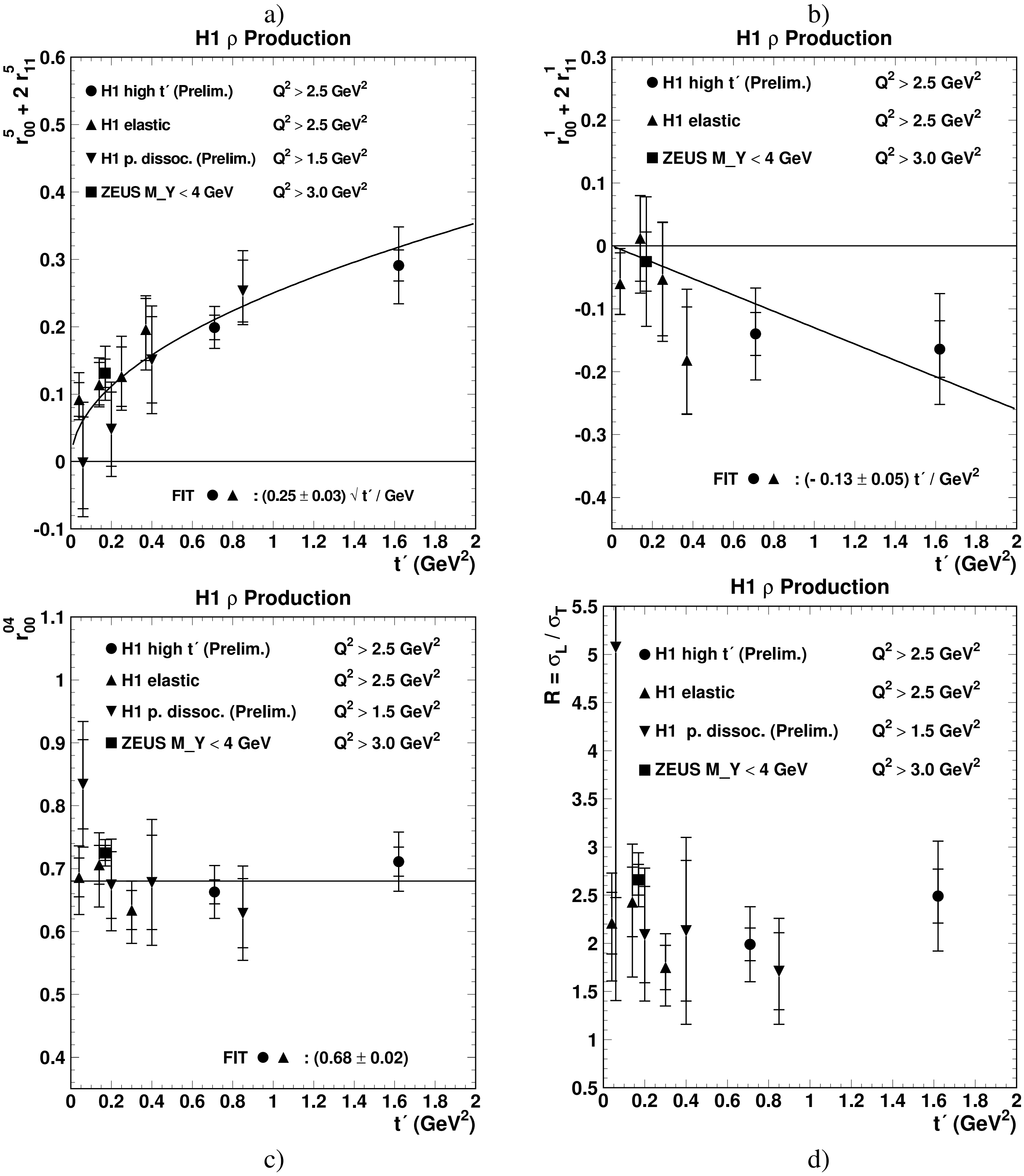

Figure 4: a) Measurement of $r^5_{00} + 2r^5_{11}$ as a function of t', for the present experiment and for ref. [1, 2, 4]; the curve presents the result of a fit of the form $r^5_{00} + 2r^5_{11} = (0.25 \pm 0.03)\ \sqrt{t'\ [\mathrm{GeV}^2]}$; b) Measurement of $r^1_{00} + 2r^1_{11}$ as a function of t', for the present experiment and for ref. [1, 2]; the curve presents the result of a linear fit with the slope parameter $-0.13 \pm 0.05\ \mathrm{GeV}^{-2}$; c) Measurement of r^{04}_{00} as a function of t', for the present experiment and for ref. [1, 2, 4]; the curve presents the result of a constant fit with $r^{04}_{00} = 0.68 \pm 0.02$; d) $R = \sigma_L/\sigma_T$ as a function of t', for the present experiment and for ref. [1, 2, 4]. In all plots, the inner error bars are statistical, the full error bars include the systematic errors added in quadrature. The fits are performed to the data of the present analysis and of ref. [1], which were obtained in the same Q^2 range.

density matrix element is proportional to the product of the non-dominant non-flip amplitude T_{11} by the double flip amplitude. The sign of the combination gives interesting information on the relative strength of the $T_{01}T_{01}^{\dagger}$ and $T_{11}T_{1-1}^{\dagger}$ products of amplitudes. It tends to confirm that the T_{01} amplitude is relatively large in the present kinematical domain, and is presumably the dominant single flip amplitude. A linear fit to the present measurements and those of ref. [1] gives the slope parameter $-0.13 \pm 0.05\ \mathrm{GeV}^{-2}$.

3.3 $\cos\theta^*$ distribution and r_{00}^{04} determination

The $\cos\theta^*$ distribution is given by [5]:

$$W(\cos\theta^*) \propto 1 - r_{00}^{04} + (3\, r_{00}^{04} - 1) \cos^2\theta^*. \tag{12}$$

Fig. 3e-f presents the fully corrected $\cos\theta^*$ distributions for the two bins in t'. The amount of background was fixed by the iterative procedure described above, and the shape of this background was taken as flat. This was obtained in the data itself from the difference in shape of the $\cos\theta^*$ experimental distributions for the events with $\zeta < 0$ and $\zeta > 0$, which contains different background contributions, these two samples being predicted by the ρ simulation to have the same $\cos\theta^*$ distributions. Systematic uncertainties were taken into account in the same way as for the Φ distribution; in the present case, the shape of the background was varied by supposing that it has the same distribution as the ρ signal.

The r_{00}^{04} element was also extracted using the events with $\zeta < 0$, where the background is small. The results are compatible with those obtained from the sample of tag events. The difference between the two measurements was included in the systematic errors.

The extracted values of r_{00}^{04} are presented in fig. 4c, together with measurements at lower t' values in the same Q^2 range. As expected from QCD calculations, no significant variation of r_{00}^{04} with t' is observed. A fit to the present measurements and to those of ref. [1] gives $r_{00}^{04} = 0.68 \pm 0.02$.

The measurement of r_{00}^{04} yields a determination of $R = \sigma_L/\sigma_T$ through the relation

$$R = \frac{1}{\epsilon} \frac{r_{00}^{04}}{1 - r_{00}^{04}}, \tag{13}$$

which is valid in the approximation of *s*-channel helicity conservation (the small SCHC violation implies an overestimate of the value of *R* with a few %). Results are shown in fig. 4d.

4 Conclusion

A measurement has been performed of ρ meson production in the t' range $0.5 < t' < 3.0\ \mathrm{GeV}^2$, for $Q^2 > 2.5\ \mathrm{GeV}^2$ and $40 < W < 120$ GeV. The r_{00}^{04} density matrix element and the combinations $r_{00}^{5} + 2r_{11}^{5}$ and $r_{00}^{1} + 2r_{11}^{1}$ have been measured as a function of t'.

No significant t' dependence has been observed for r_{00}^{04}.

A significant violation of s-channel helicity conservation is observed in the $r^5_{00} + 2r^5_{11}$ combination, which is increasing with t'. The t' dependence of the combination has been determined for the first time as $r^5_{00} + 2r^5_{11} = (0.25 \pm 0.03)\ \sqrt{t'}$, with t' in GeV^2.

The $r^1_{00} + 2r^1_{11}$ element combination appears to be different from zero and negative. This is the first observation of a non-zero value of this combination. The sign gives interesting information on the relative strength of the $T_{01}T^{\dagger}_{01}$ and $T_{11}T^{\dagger}_{1-1}$ products of amplitudes. Together with the $r^5_{00} + 2r^5_{11}$ measurement, it tends to confirm that the T_{01} amplitude is relatively large in the present kinematical domain, and is presumably the dominant helicity flip amplitude.

Acknowledgements

We are grateful to the HERA machine group whose outstanding efforts have made and continue to make this experiment possible. We thank the engineers and technicians for their work in constructing and now maintaining the H1 detector, our funding agencies for financial support, the DESY technical staff for continual assistance, and the DESY directorate for the hospitality which they extend to the non-DESY members of the collaboration.

References

[1] H1 Collab., C. Adloff et al., *Eur. Phys. J.* **C13** (2000) 371.

[2] ZEUS Collab., J. Breitweg et al., *Eur. Phys. J.* **C12** (2000) 393 ;
ZEUS Collab., J. Breitweg et al., *Eur. Phys. J.* **C6** (1999) 603.

[3] H1 Collab., C. Adloff et al., *Phys. Lett.* **B483** (2000) 360 ;
ZEUS Collab., M. Derrick et al., *Phys. Lett.* **B380** (1996) 220.

[4] J. Olsson, H1 Collab., proc. of the DIS2001 workshop, Bologna, Italy, 2001.

[5] K. Schilling and G. Wolff, *Nucl. Phys.* **B61** (1973) 381.

[6] D.Yu. Ivanov and R. Kirchner, *Phys. Rev.* **D58** (1998) 114026.

[7] E.V. Kuraev, N.N. Nikolaev and B.G. Zakharov, *JETP Lett.* 68 (1998) 696.

[8] I. Royen, hep-ph/0006044 ;
I. Royen and J.R. Cudell, *Nucl. Phys.* **B545** (1999) 505.

[9] Review of Particle Physics, *Eur. Phys. J.* **C15** (2000) 1.

[10] DIFFVM program, B. List, *Diploma Thesis*, Tech. Univ. Berlin, unpublished (1993).

[11] HERACLES 4.4 , H. Spiesberger, unpublished manual program (1993).

[12] ZEUS Collab., J. Breitweg et al., *Phys. Lett.* **B487** (2000) 273.

[13] MINUIT, Cern Program Library Long Writeup D506.

[14] M. Ross and L. Stodolsky, *Phys. Rev.* **149** (1966) 1173.